Available online www.jsaer.com

***Journal of Scientific and Engineering Research*, 2017, 4(8):342-359**

Research Article

ISSN: 2394-2630
CODEN(USA): JSERBR

An investigation of stress-strain distribution of an elastic thin cylindrical panel under lateral pressure

S. Jafari*

Mechanical Engineering Department, University of Bojnord, Bojnord, Iran

Abstract In this paper a three dimensional semi-analytical model is developed to estimate the elastic limit capacity and distribution of displacement, stress and strain components of cylindrical panel subjected to uniformly pressure distribution on the external surface. The Flugge second-order approximation of thin shell theories in general form with Navier type formulations of equilibrium equations is considered. Governing equations of the cylindrical panel are solved using higher order finite difference technique that converts them to a system of linear equations. Furthermore, the Richardson extrapolation technique is used to improve the accuracy of results in the semi-analytical method. Results obtained by the semi-analytical method are compared and verified by the finite element method. Parametric studies are carried out for different values of the total angle, the mean radius and the wall thickness (ϕ_0, R, h) of the panel by validated semi-analytical method. The results of semi-analytical method can be used for simulating contact pressure due to indentation process in both elastic and plastic deformations of panel with different indenter shape, boundary and geometry conditions.

Keywords Thin cylindrical panel, elastic limit capacity, Navier method, Finite difference method, Richardson extrapolation technique, semi-analytical method

Introduction

Engineering equipment frequently rely on the integrity of components with interacting surfaces under the effect of high contact pressures and stresses. It is an engineering requirement to design components to withstand such high contact stresses [1-4]. The problems of cylindrical panels under external loadings have been treated extensively in the past due to their wide application in civil, mechanical, aeronautical and marine engineering [5]. As can be seen in the literature, the governing theories of thin cylindrical shells such as those presented by Sanders [6], Flugge [7], Love [8]-Timoshenko [9], Niordson [10], Donnell [11]-Mushtari [12], Vlasov[13]etc, are used for the analysis of thin cylindrical panels [5].

In the field of cylindrical shells, Huble [14] worked on the analytical elastic-plastic solution of cylindrical shells under axisymmetric loading conditions. The analytical solution was reduced to an ordinary nonlinear differential equation of the order four. Yi et al. [15] investigated the elastic solution for a cylindrical shell subjected to a symmetric, partially distributed and self-balanced radial pressure loading by a dual series approach assuming the plane strain condition. Tooth et al. [16] examined the behavior of a cylindrical vessel loaded by a rigid attachment of rectangular form. Equilibrium equations according to the Sander's theory for cylindrical shell were solved using double Fourier series expansion technique. The stresses induced by interfacial forces are found to be 37% higher than those of a uniformly distributed force on the external surface of the vessel. Alijani et al. [17] studied the bending problem of clamped cylindrical panels using the extended Kantorovich method to obtain highly accurate approximation to the closed form solution for uniform and non-uniform loading condition. Free vibration analysis of functionally graded (FG) curved thick panels under various boundary conditions based on the three-dimensional elasticity theory was studied by Zahedinejad et al [18]. In the field of

finite element analysis, Salahifar et al. [19] worked on the super convergent finite element solution for the steady state simulation of a circular cylindrical shell under general harmonic forces based on the thin shell theory. Weicker et al. [20, 21] investigated on the development of governing equilibrium equations and boundary conditions by principle of virtual work for a thin-walled pipe subjected to general loading. The founding of this paper was used to develop a finite element formulation for stress-deformation analysis of long pipes [20, 21].

This paper presents a semi-analytical model to analyze the behavior of a thin cylindrical panel under the effect of pressure loading on the external surface. The distribution of pressure is assumed to be uniform in semi-rectangular area and components of the deformation vector in the cylindrical panel are calculated using the Navier formulations of the thin shell theory. The von Mises yield criterion is assumed as the yield criterion of the material for prediction of the elastic limit load. Three dimensional equilibrium equations, strain-displacement relations, force and moment resultants are described using the presented thin shell theories. Higher order finite difference method is proposed to solve the three dimensional Navier equilibrium equations. The Doolittle LU factorization inverse method is used to solve the linear system of equations. For verification presented semi-analytical method; the uniformly distributed pressure loading is applied to semi-rectangular area on one panel with specified geometric parameters until the plastic deformation starts. The convergence tests are done and the Richarson extrapolation technique is employed to reduce the computational time and size. The results obtained by the semi-analytical method are compared with those obtained by the finite element method. Secondly and to carry out numerical calculations, different panel dimensions with constant arc length and different mean radii, total panel angles and wall thicknesses are considered for numerical calculation and parametric study. Two opposite edges of the panels are considered to be simply supported and the other two clamped. The panel is assumed to be made of 2024-T351 Aluminum alloy. The material properties of the panel under study in this research are shown in Table 1.

Table 1: Material properties of the cylindrical panel

E (GPa)	E_t (GPa)	ν	$\sigma_\circ$ (MPa)	$\rho_\circ$ (kg/m^3)
70	35	0.3	300	2800

Governing equations

A thin cylindrical panel with constant thickness (h) mean radius (R) axial length (L) Poisson's ratio (ν) density (ρ) and Young's modulus of elasticity (E) is considered. The shell is assumed to be thin (*i.e.* $h/R\langle\langle 1$). The panel geometry is defined in the cylindrical coordinate system (x,ϕ,z), where x and ϕ are the axial and circumferential directions of the shell and z is perpendicular to the middle surface pointing outward, i.e. $-h/2 \le z \le h/2$, as shown in Fig.1. The origin of the coordinate system is taken at one end of the cylindrical panel. A plane stress state for the thin cylindrical panel is considered, i.e the stress components in the z direction of the panel is assumed to be zero ($\tau_{z\phi},\tau_{zx},\sigma_z = 0$).The respective displacements in the axial, circumferential and radial directions are demonstrated by $u(x,\phi)$, $v(x,\phi)$ and $w(x,\phi)$.

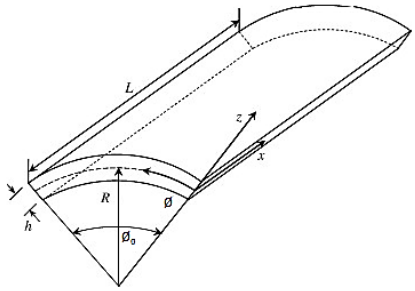

Figure 1: Panel dimensions and cylindrical coordinates

Equilibrium equations

In order to carry out the analysis of the thin cylindrical panel under external loading condition, all equilibrium equations consisting of bending and shear stress components according to the general theory of the thin shell are considered. As it is well explained in [7, 10], the equilibrium equations are developed on the basis of the resultant forces and moments of the middle surface of the shell. By eliminating the transverse shear stresses from these equations, the equilibrium equations of a cylindrical shell under distributed radial loading, i.e. ($p_z(x,\phi)$) based on the Flugge shell theory are given by [7, 10]:

$$R\frac{\partial N_x(x,\phi)}{\partial x}+\frac{\partial N_{\phi x}(x,\phi)}{\partial \phi}=0 \tag{1}$$

$$R^2\frac{\partial N_{x\phi}(x,\phi)}{\partial x}+R\frac{\partial N_{\phi}(x,\phi)}{\partial \phi}-\frac{\partial M_{\phi}(x,\phi)}{\partial \phi}-R\frac{\partial M_{x\phi}(x,\phi)}{\partial \phi}=0 \tag{2}$$

$$R\frac{\partial^2 M_{x\phi}(x,\phi)}{\partial x\partial \phi}+R\frac{\partial^2 M_{\phi x}(x,\phi)}{\partial x\partial \phi}+\frac{\partial^2 M_{\phi}(x,\phi)}{\partial \phi^2}+R^2\frac{\partial^2 M_x(x,\phi)}{\partial x^2}+R\,N_{\phi}(x,\phi)+p_z(x,\phi)R^2=0 \tag{3}$$

$$RN_{x\phi}(x,\phi)-RN_{\phi x}(x,\phi)+M_{\phi x}(x,\phi)=0 \tag{4}$$

where $(N_x, N_\phi, N_{x\phi}, N_{\phi x})$ are the force resultants, $(M_x, M_\phi, M_{x\phi}, M_{\phi x})$ are the moment resultants. It can be seen from above equations that in general for a cylindrical shell, $N_{x\phi}\neq N_{\phi x}$ and $M_{x\phi}\neq M_{\phi x}$.

Resultant forces and moments

In the Flugge second-order approximation of thin shell theories, the non-dimensional term, z/R_i (where $R_i, i=1,2$ are the radii of curvature of the middle surface), is taken into account for computation of the resultant forces, moment integrals and strain relations. The internal force and moment resultants can be calculated by integrating the stress distribution through the shell thickness [8]. These resultants in the plane stress conditions are expressed in integral terms of the stress components through the thickness of the shell as reported in [5, 7, 10]:

$$\begin{Bmatrix} N_x(x,\phi)\\ N_{x\phi}(x,\phi)\\ M_x(x,\phi)\\ M_{x\phi}(x,\phi)\end{Bmatrix}=\int_{-\frac{h}{2}}^{\frac{h}{2}}\begin{Bmatrix}\sigma_x(x,\phi)\\ \tau_{x\phi}(x,\phi)\\ -z\sigma_x(x,\phi)\\ -z\tau_{x\phi}(x,\phi)\end{Bmatrix}(1+\frac{z}{R})dz,\quad \begin{Bmatrix} N_\phi(x,\phi)\\ N_{\phi x}(x,\phi)\\ M_\phi(x,\phi)\\ M_{\phi x}(x,\phi)\end{Bmatrix}=\int_{-\frac{h}{2}}^{\frac{h}{2}}\begin{Bmatrix}\sigma_\phi(x,\phi)\\ \tau_{x\phi}(x,\phi)\\ -z\sigma_\phi(x,\phi)\\ -z\tau_{x\phi}(x,\phi)\end{Bmatrix}dz \tag{5}$$

where σ_x and σ_ϕ are the axial and circumferential stresses, $\tau_{x\phi}$ is the shear stress. By performing such integrations, the variations with respect to z are eliminated and the three dimensional problem of the cylindrical shell reduces to a two degree problem of deformation of the middle surface of the shell.

Stress-strain relations

The stress-strain relations in an isotropic material under the elastic deformation are expressed with the help of two material constants namely the Poisson's ratio and the Young's modulus of elasticity. Hence, the stress-strain relations for the plane stress condition are [5, 7, 10]:

$$\sigma_x(x,\phi)=\frac{E}{(1-\nu^2)}\left[\varepsilon_x(x,\phi)+\nu\varepsilon_\phi(x,\phi)\right] \tag{6}$$

$$\sigma_\phi(x,\phi)=\frac{E}{(1-\nu^2)}\left[\varepsilon_\phi(x,\phi)+\nu\varepsilon_x(x,\phi)\right] \tag{7}$$

$$\tau_{x\phi}(x,\phi)=\frac{E}{2(1+\nu)}[\gamma_{x\phi}(x,\phi)] \tag{8}$$

where ε_x and ε_ϕ are the total normal strains and $\gamma_{x\phi}$ is the shear strain component.

Strain-displacement relations

The total strain of an element of the shell located at a distance z from the middle surface consists of two parts, namely the membrane strain and the strain due to the curvature [7, 10]. Hence, the total strain considering the term z / R_i for the cylindrical panel is obtained as follow [5]:

$$\varepsilon_x(x,\phi) = \frac{1}{(1+z/R_1)}[\bar{\varepsilon}_x(x,\phi) + z\chi_x(x,\phi)] \tag{9}$$

$$\varepsilon_\phi(x,\phi) = \frac{1}{(1+z/R_2)}[\bar{\varepsilon}_\phi(x,\phi) + z\chi_\phi(x,\phi)] \tag{10}$$

$$\gamma_{x\phi}(x,\phi) = \frac{1}{(1+z/R_1)(1+z/R_2)}[\bar{\gamma}_{x\phi}(1-z^2/R_1R_2) + 2z\chi_{x\phi}(1-\frac{z}{2}(1/R_1+1/R_2))] \tag{11}$$

where $\bar{\varepsilon}_x$ and $\bar{\varepsilon}_\phi$ are the normal strains, $\bar{\gamma}_{x\phi}$ is the shear strain at the middle surface of the shell, and $\chi_x, \chi_\phi, \chi_{x\phi}$ are the curvatures. With considering curvature radii for the cylindrical panel as $R_1 = \infty, R_2 = R$, above relations can be redefined as follow [5]:

$$\varepsilon_x(x,\phi) = [\bar{\varepsilon}_x(x,\phi) + z\chi_x(x,\phi)] \tag{12}$$

$$\varepsilon_\phi(x,\phi) = \frac{1}{(1+z/R)}[\bar{\varepsilon}_\phi(x,\phi) + z\chi_\phi(x,\phi)] \tag{13}$$

$$\gamma_{x\phi}(x,\phi) = \frac{1}{(1+z/R)}[\bar{\gamma}_{x\phi} + 2z\chi_{x\phi}(1-\frac{z}{2}(1/R))] \tag{14}$$

It is observed that as the wall thickness of the cylindrical shell reduces, the ratio of z / R_i becomes smaller and its effect in strain relations approaches to zero. A quick review of research works on thin shells reveals that the same expressions are used for the membrane strains; however different expressions for the curvature strain are defined, depending on the simplifying assumptions and the solution treatment. In this research, the Niordson formulations of curvature strains are employed for analytical modeling of the cylindrical panel. According to the Niordson's shell theory, strains and curvatures of the middle surface are related to the displacement components (w,u,v) in the (x,ϕ,z) coordinate directions as follow [10]:

Membrane strains:

$$\bar{\varepsilon}_x = \frac{\partial u(x,\phi)}{\partial x}$$

$$\bar{\varepsilon}_\phi = \frac{1}{R}\frac{\partial v(x,\phi)}{\partial \phi} + \frac{w(x,\phi)}{R}$$

$$\bar{\gamma}_{x\phi} = (\frac{1}{R}\frac{\partial u(x,\phi)}{\partial \phi} + \frac{\partial v(x,\phi)}{\partial x}) \tag{15}$$

Curvatures:

$$\chi_x = -(\frac{\partial^2 w(x,\phi)}{\partial x^2})$$

$$\chi_\phi = -\frac{1}{R^2}(\frac{\partial^2 w(x,\phi)}{\partial \phi^2} - 2\frac{\partial v(x,\phi)}{\partial \phi} + w(x,\phi))$$

$$\chi_{x\phi} = -\frac{1}{R}(\frac{\partial^2 w(x,\phi)}{\partial x \partial \phi} - \frac{1}{2}\frac{\partial v(x,\phi)}{\partial x}) \tag{16}$$

Finite element model

A numerical procedure based on the finite element method is developed to estimate the elastic limit load and displacement, stress and strain components of the cylindrical panel subjected to uniformly pressure distribution on the external surface. It comprises of a nonlinear three dimensional shell type elastic-plastic model developed

employing the ANSYS suite of program [22]. Finite element method that used in this research is verified by the author in the previous papers by experimental results [23-27]. The cylindrical panel with diameter of the middle surface (R) the wall thickness (h) and the total angle (ϕ_0) is modeled and meshed using 4-noded shell element, namely SHELL181 with six degrees of freedom at each node. The von Mises yield criterion with isotropic hardening effect is assumed as the yield criterion of the material for prediction of the elastic limit load. The material is assumed to have bilinear strain hardening behavior that is defined according to the stress-strain data curve using the TB, BISO commands, as shown in Fig. 2. The loading condition is implemented on the outer surface of the panel with surface load command. The value of the applied load is increased until the equivalent von Mises stress of the panel reaches the yield strength of the material of the panel. Once the loading reaches the limit load, plastic flow begins and the plastic deformation occurs in the cylindrical panel. Simply supported-clamped boundary conditions are applied at the opposite edges of the panel, respectively.

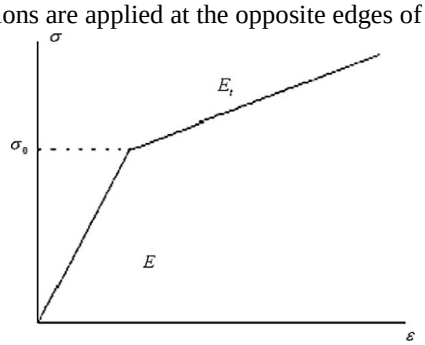

Figure 2: Idealized stress–strain curve for a linear hardening material

Due to symmetry in the geometry and the loading of the cylindrical panel, it is desirable to model just a quarter of the panel in order to reduce both the model size and the solution timing. An example of the boundary, symmetry and loading conditions and the finite element meshing for the cylindrical panel is shown in Fig. 3. A convergence test is also carried out to obtain the appropriate number of elements for the analysis of the cylindrical panel.

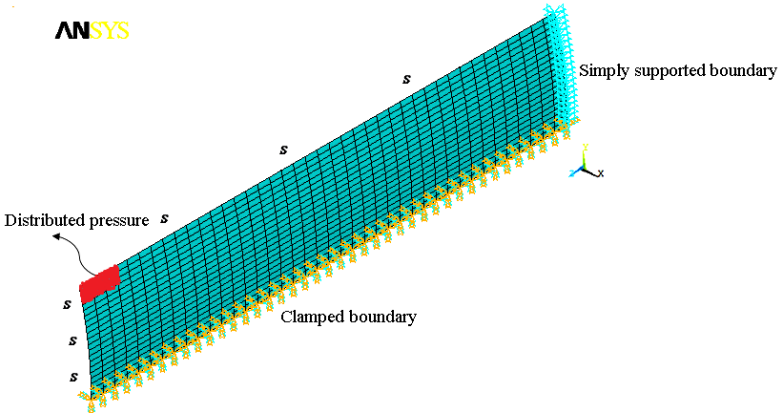

Figure 3: Finite element model of the cylindrical panel

Semi-analytical method (SAM)

In this section, the effective semi-analytical method for the analysis of the cylindrical panel under distributed pressure load is presented.

Navier formulation

The Navier type formulation is developed by substituting the components of the displacement of the middle surface and their derivatives in the equilibrium equations. The components of the displacement which are obtained by the Navier method satisfy the strain compatibility relations. The strain-displacement relations (15) and (16) are substituted in strain relations, (12-14) and the results are further substituted in the stress-strain relations (6-8). The force and moment resultants are computed with the help of Eq. (5) and the expressions are substituted into the equations of equilibrium that reduces the problem into a set of simultaneous linear

differential equations with respect to the *x* and ϕ. The governing partial differential equation of the cylindrical shell in Navier form is shown in appendix A. As shown in the appendix A, the fourth equilibrium equation is automatically satisfied for the proposed constitutive relations and kinematic equations. Therefore, the number of governing differential equations of the cylindrical shell is reduced to a system of equations consisting of two second order and one fourth order equations with three unknown displacements components, i.e. u, v, w. In the next section, the governing differential equations are solved with the help of higher order finite difference method. Distribution of the pressure is included in the third equilibrium of equation in Appendix A, for the specified range in x and ϕ directions of the cylindrical panel.

Higher order finite difference method (HFDM)

It is obvious that the system of differential equations for the thin cylindrical shell cannot be solved analytically. So the only possible way is to solve the problem using a numerical method, among which the finite difference method (FDM) is found to be one of the most effective. In FDM the derivatives appearing in the differential equation and boundary conditions are replaced by suitable finite difference approximations. The accuracy of the solution depends on the number of grid points. One can increase the accuracy of the solution to some desired degree by increasing the number of grid points. However, it involves increasingly tedious mathematical analysis. To obtain a sufficiently accurate solution of the problem under study, higher order finite difference formulations are used in this research. Li [28] and Ashok et al [29] presented a general explicit difference formula with arbitrary order of accuracy for approximating the first and higher order derivatives that can be used for both equally and unequally spaced grid nodes. In this research, the fourth-order FD approximations in two dimensions are used for difference approximations to the governing differential equations of the cylindrical panel. To achieve the constant error in computations ($O(h^4)$), 5 points for first and second order derivatives and 7 points for the third and fourth orders are used for FD approximations. As an example, the fourth-order approximation of the first derivative of a function $u(x,\phi)$ with respect to x in the central difference form can be written as [29]:

$$\left.\frac{du(x,\phi)}{dx}\right|_{x=x_i,\phi=\phi_j} = \frac{-u_{i+2,j}+8u_{i+1,j}-8u_{i-1,j}+u_{i-2,j}}{12\Delta x}+O(h^4) \tag{17}$$

When higher-order approximations are used at and near the boundary, nodes outside of the domain would be needed. Therefore the forward and backward scheme of higher order FD form is included to differential equations for these nodes. The forward and backward formulation of the first derivative of a function $u(x,\phi)$ with respect to x can be written as [29]:

Forward:

$$\left.\frac{du(x,\phi)}{dx}\right|_{x=x_i,\phi=\phi_j} = \frac{-u_{i+2,j}+4u_{i+1,j}-3u_{i,j}}{2\Delta x}+O(h^2) \tag{18}$$

Backward:

$$\left.\frac{du(x,\phi)}{dx}\right|_{x=x_i,\phi=\phi_j} = \frac{u_{i-2,j}-4u_{i-1,j}+3u_{i,j}}{2\Delta x}+O(h^2) \tag{19}$$

Implementation of HFDM

A finite difference method for solving the differential equations basically involves four steps [28, 30]:

1. Dividing the problem domain into grids of nodes by equally or unequally spaced scheme.
2. Approximating the given differential equation by the finite difference equivalence that relates the solutions to grid nodes.
3. Writing the difference equations for each grid nodes and to the prescribed boundary conditions and/or initial conditions.
4. Solving the system of linear equations obtained by an appropriate method.

According to appendix A, the governing differential equations of the cylindrical panel have two dimensions, hence the panel is divided by N nodes in the *x*-direction ($i=[1,N]$) and M nodes in ϕ-direction ($j=[1,M]$). The higher order FD formulation corresponding to the developed Navier form of differential equilibrium equations can be found in Appendix B. For each grid node in the 2D domain of the cylindrical panel, the differential equations are written in the FD form. Also, the boundary conditions which are explained in the next section are written for boundary nodes in the FD scheme. The number of interior nodes for which the set of differential equations can be written is $(N-2)(M-2)$ and the numbers of unknown interior displacements which must be calculated are $3(N-2)(M-2)$. The results of finite element simulations show that components of displacement in the cylindrical panel have symmetry conditions as shown in Fig. (4) [23-27]. These symmetry conditions are due to the symmetry of the boundary conditions and distribution of the pressure in the cylindrical panel. These conditions can be used for developing semi-analytical model in the quarter model of the cylindrical panel. As seen in Fig. (4), the unknown components of displacement for considered quarter model of the cylindrical panel is proposed as $w_{i,j},u_{i,j},v_{i,j}$ for $i=[1,(N+1)/2]$and $j=[1,(M+1)/2]$.The values of displacement components for other quarters are defined on the basis of the assumed set, i.e. $w_{i,j},u_{i,j},v_{i,j}$. Finally, the number of unknown displacements is reduced to $3((N-1)/2)((M-1)/2)$ and the set of $3((N-1)/2)((M-1)/2)$ linear algebraic equations can be obtained in the following matrix expression that must be solved using an appropriate method.

$$A\cdot x=b \tag{20}$$

In this relation $A_{p,q},\ p=q=3((N-1)/2)((M-1)/2)$ is the coefficient matrix of the linear system of equations which is square and symmetric. The vector b_p corresponds to the value of distributed pressure loading for each node and x_q is the vector containing the displacement components $w_{i,j},u_{i,j},v_{i,j}$. The Doolittle LU factorization method is used to inverse the coefficient matrix *A* and solves the linear system of equations in FD form. This method is used to solve the equation with less number of required multiplications in comparison with other inverse methods. More detailed information about Doolittle LU factorization method can be found in references [31]. The Richarson extrapolation technique is employed to reduce the size and time of computation with the expected order of accuracy that is described in the next section.

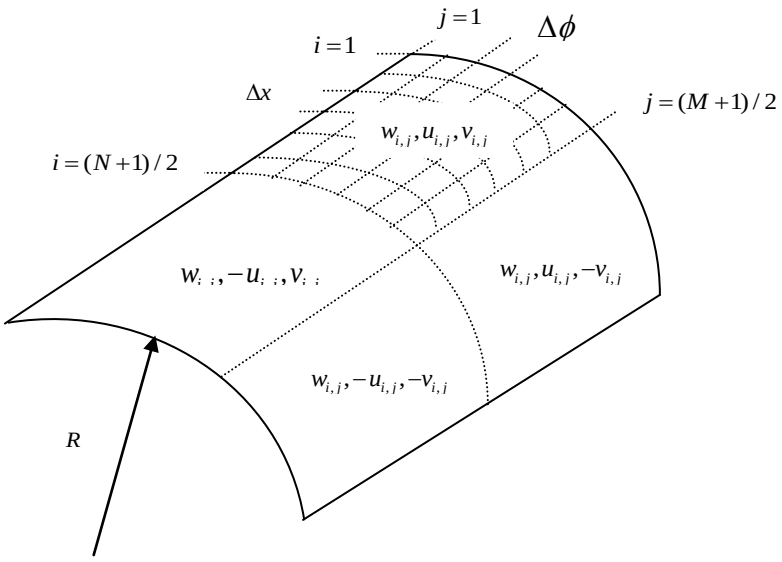

Figure 4: Finite difference grid nodes and symmetry condition

Richardson extrapolation method

Richardson's extrapolation is used to generate high accuracy results while using low order formulas grid nodes [32]. Improved accuracy can be obtained by solving the same problem with different grid sizes and extrapolating the results to zero order grid size. In order to apply the Richarson extrapolation in FD solution of differential equations the following stages must be considered [32-34]:

1- First approximate the truncation error of FD formula: in the fourth-order FD the truncation error is $O(h^4)$ [33].

2- Create the coarse grid nodes with interval of h and use finer grid nodes until the required convergence is achieved. Variation of the grid node distance at each step, i.e. step k, is shown below.

$$h_k = h_{k-1}/2 \rightarrow h_1 = h,\ h_2 = h_1/2,\ h_3 = h_2/2,.... \tag{21}$$

3- Based on the truncation error of FD form which is used in the problem, the corresponding of Richardson formula is employed as [32-34]:

$$R_{k,j} = R_{k,j-1} + \frac{R_{k,j-1} - R_{k-1,j-1}}{4^{j-1}-1} \quad (O(h^{2j}),\ j \geq 1) \tag{22}$$

It is worth mentioning that the rate of convergence in this method is high and the solution algorithm is simple.

Boundary conditions

We assume that the shell is simply supported at the edges $x = 0, x = L$ and calmed at the edges $\phi = 0, \phi = \phi_0$ .For the simply supported edge, i.e. $x = 0$, the BC's may be written as:

$w(0,\phi) = 0,\ u(0,\phi) = 0,\ v(0,\phi) = 0,\ M_x(0,\phi) = 0$

Using the integral form of $M_x(x,\phi)$ as defined in Eq. (5), the final form of $M_x(x,\phi)$ is defined as:

$$M_x(x,\phi) = \frac{Eh^3}{12(\nu^2-1)R^2}\left[-\frac{\partial^2 w(x,\phi)}{\partial x^2}R^2 + \frac{\partial u(x,\phi)}{\partial x}R + 2\frac{\partial v(x,\phi)}{\partial \phi}\nu - w(x,\phi)\nu - \frac{\partial^2 w(x,\phi)}{\partial \phi^2}\nu\right] \tag{23}$$

Along the considered edges, x =constant, the corresponding derivatives with respect to ϕ are zero. Thus, the above equation becomes:

$$M_x(0,\phi) = \frac{Eh^3}{12(\nu^2-1)R^2}\left[-\frac{\partial^2 w(0,\phi)}{\partial x^2}R^2 + \frac{\partial u(0,\phi)}{\partial x}R\right] = 0 \tag{24}$$

The FD form of Eq. (25) can be obtained by using the ordinary FD relations as:

$$M_x(0,\phi) = -\frac{w_{i+1,j} - 2w_{i,j} + w_{i-1,j}}{\Delta x^2}R^2 + \frac{u_{i+1,j} - u_{i,j}}{\Delta x}R = 0 \rightarrow \frac{w_{i+1,j} - 2w_{i,j} + w_{i-1,j}}{\Delta x^2} = \frac{u_{i+1,j} - u_{i,j}}{R\Delta x} \tag{25}$$

This set of boundary conditions is written for $x = 0$ or $i = 1$ in the FD form as follow:

$$w(1,j) = 0,\ u(1,j) = 0,\ v(1,j) = 0,\ \frac{w_{2,j} - 2w_{1,j} + w_{2,j}}{\Delta x^2} = \frac{u_{2,j} - u_{1,j}}{R\Delta x}$$

The simply supported BC of the edge $x = L$ or $i = N$ is written in a similar manner of $x = 0$. For the clamped boundary condition of the edge $\phi = 0$, one can write:

$$w(x,0) = 0,\ u(x,0) = 0,\ v(x,0) = 0,\ \frac{\partial w(x,0)}{\partial \phi} = 0$$

The FD form of boundary condition for $\frac{\partial w(x,0)}{\partial \phi} = 0$ can be obtained by using the ordinary FD as:

$$\frac{w_{i,j+1} - w_{i,j-1}}{2\Delta\phi} = 0 \ \rightarrow w_{i,j+1} = w_{i,j-1} \tag{26}$$

This set of boundary conditions is expressed for $\phi = 0$ or $j = 1$ in FD form as follow:

$w(i,1) = 0,\ u(i,1) = 0,\ v(i,1) = 0,\ w(i,0) = w(i,2)$

The clamped BC for the edge $\phi = \phi_0$ or $j = M$ is written in a similar manner as of $\phi = 0$.

Numerical Results and Discussion

The semi-analytical method outlined in the previous sections can be used to obtain highly accurate solutions for any type of pressure distribution and contact area on the cylindrical panel. Dimensions of the panels for the numerical calculation and parametric study are presented in Table 2 indicating the constant arc length panels with different mean radius, total panel angle and wall thickness. As mentioned earlier, all models of the panel specified in Table 2, have two simply supported and two clamped boundaries. The opposite edges of the panel have the same boundary conditions. The von Mises yield criterion is considered for estimation of the elastic limit load at which plastic deformation occurs.

The panel model $P3$ in Table 2 has special geometric dimensions with maximum total angle and minimum wall thickness in comparison with other proposed models. The convergence test of FE simulation and semi-analytical method are concerned on determination of the elastic limit capacity, distribution of displacement components and the von Mises stress for this panel model. For better understanding of the verification process of the presented semi-analytical method, a uniformly distributed pressure is applied over a semi-rectangular area on the external surface of the panel model $P3$ as specified in Table 3.The value of the uniformly distributed pressure on the considered small area that causes the von Mises stress reaching the yield strength of the material ($\sigma_e = 300MPa$) is considered as P_e.

Table 2: Geometric dimensions of the proposed cylindrical panel model

Model	$\widehat{S} = R\phi_0$	ϕ_0	R (m)	h (m)	h/R	L (m)
$P1$	0.1950	30°	0.37225	0.015	0.04	1
$P2$	0.1950	30°	0.37225	0.012	0.032	1
$P3$	0.1950	30°	0.37225	0.01	0.026	1
$P4$	0.1950	22.5°	0.4963	0.01	0.02	1
$P5$	0.1950	15°	0.7445	0.01	0.013	1

Table 3: Pressure distribution for different panel models

Model	$p_z(x,\phi)$	Range of loading along the X: Δx	Range of loading along the ϕ: $\Delta\phi$
$P1$	p_0	$0.4 \le x \le 0.6$	$12^\circ \le \phi \le 18^\circ$
$P2$	p_0	$0.4 \le x \le 0.6$	$12^\circ \le \phi \le 18^\circ$
$P3$	p_0	$0.4 \le x \le 0.6$	$12^\circ \le \phi \le 18^\circ$
$P4$	p_0	$0.4 \le x \le 0.6$	$9^\circ \le \phi \le 13.5^\circ$
$P5$	p_0	$0.4 \le x \le 0.6$	$6^\circ \le \phi \le 9^\circ$

All results in this research are compared for the paths defined in the axial and circumferential directions as shown in the Table 4.

Table 4: Path range for displacing results on the proposed panel models.

Path number	Range of path along the X direction	Range of path along the ϕ direction
1	$0 \le x \le L$	$\phi = \phi_0 / 2$
2	$x = L/2$	$0^\circ \le \phi \le \phi_0$

The convergence test of Finite element method

The FE simulations are carried out for the quarter model of the panel on the basis of symmetry of the loading and boundary conditions. The uniformly distributed pressure on the outer surface of the panel model $P3$, is applied for the range of $0.4 \le x \le 0.6$ and $12^\circ \le \phi \le 18^\circ$, as shown in Table 3. The FE convergence results of von

Mises stress is shown in Table 5 at the elastic limit load of $P_e = 9.8\,MPa$. The maximum value of the von Mises stress for the current loading, boundary and symmetry conditions occurs at the central node of the cylindrical panel at $x = 0.5$ and $\phi = 15^\circ$. As shown in this table, the optimum number of element considering the converged result and duration of calculation is $N = 7500$. This optimum number of elements is found to be valid for other panel models as defined in Table 2.

Table 5: FEM Convergence test for the quarter panel model $P3$ with no. of elements, $P_e = 9.8\,MPa$.

Number of element in FE mesh	von Mises stress at $x = 0.5$ and $\phi = 15^\circ$ (MPa)
N=200	288.1
N=400	295.5
N=900	296.7
N=1600	297.9
N=2500	299.1
N=4900	299.9
N=7500	300

The convergence test of semi-analytical method

In order to verify the semi-analytical method, the results of the convergence test obtained by the higher order FDM for the components of displacement and von Mises stress of the panel model $P3$ at $P_e = 9.8\,MPa$ and various number of grid nodes along the axial and circumferential directions is shown in Fig.(5). The results of the radial and axial displacement and von Mises stress for the panel model $P3$ is shown for the path 1. Due to the symmetry of boundary conditions and applied load, the values of circumferential displacement in path 1are very small and close to zero. Hence, the circumferential displacement for path 2 is shown in Fig. (5). It is shown that the optimum number of grid nodes for the quarter model of the cylindrical panel considering the converged result and the duration of the calculation is $N = 3721$. As mentioned earlier, the optimum number of gird nodes can be used for the semi-analytical model of other panel models as shown in Table 2.

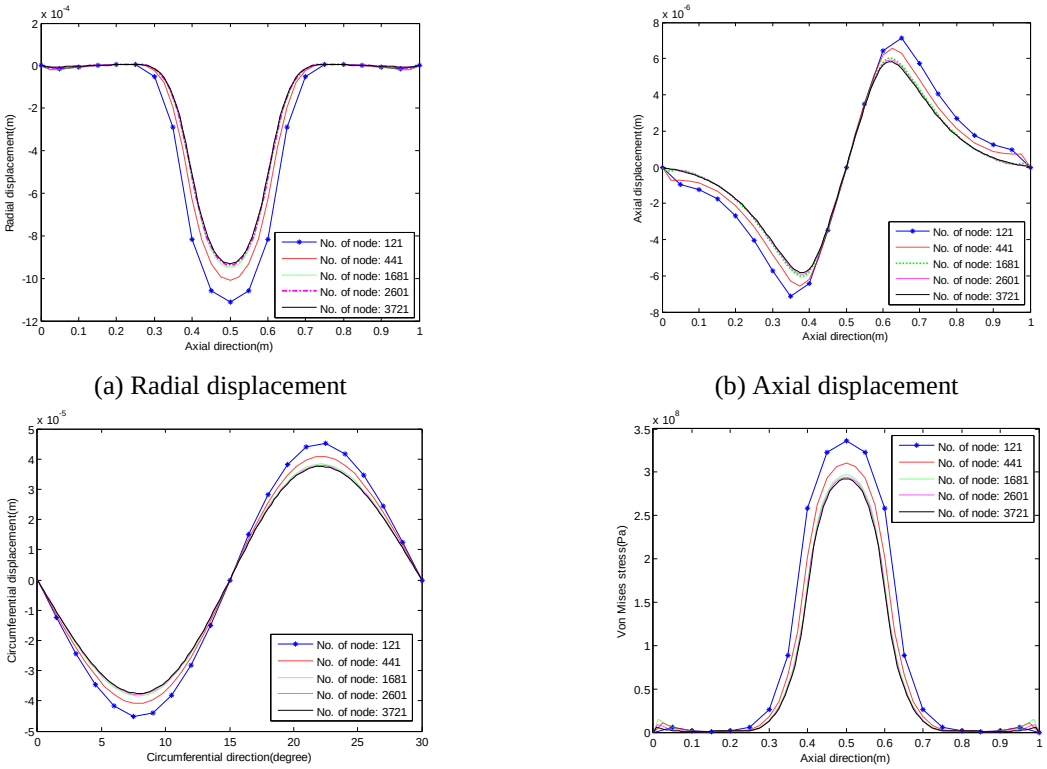

(a) Radial displacement

(b) Axial displacement

(c) Circumferential displacement

(d) Von Mises stress

Figure 5: Convergence test for higher order FDM with no. of grid nodes for the panel model $P3$ at $P_e = 9.8\,MPa$

For final validation, converged results of the semi-analytical method are compared with the corresponding results of FE simulation. Values of the radial, axial, circumferential displacements and von Mises stress at $P_e = 9.8MPa$, for the panel model $P3$ are illustrated in Fig. (6). Results are plotted for the same paths and optimum number of elements and nodes for FEM and semi-analytical methods used in Fig. (5). As shown in Fig. (6), two methods can very well describe the elastic behavior of the cylindrical panel under distributed pressure loading and are in good agreement. It can be observed that the von Mises stress σ_e reaches its maximum value at the center node of the cylindrical panel where the yielding begins. The agreement observed between results obtained by these two methods, indicates the ability of these methods to simulate the elastic deformation of the cylindrical panel in its general form. Moreover, this comparison can be made for other proposed panel models as listed in Table 2.

In the following, the Richardson extrapolation method is employed to increase the accuracy and reduce the computation time of semi-analytical method. For this, the number of nodes in x and ϕ directions must be defined in a manner that Eq. (21) is satisfied. The required grid nodes with special interval in x and ϕ directions for the panel model $P3$ are shown in Table 6. As an example, the relation governing the Richardson extrapolation for radial displacement ($w_{i,j}$) is shown in Eq. (27). By carrying out the extrapolation, the order of truncation error is increased from 4 to8. The results of Richardson extrapolation is obtained on the basis of lower number of grid nodes. For internal points, the results can be estimated by an appropriate interpolations formula.

$$\left(w_{i,j}\right)_1 = \left[w_{i,j}\right]_{N=M=41} + \frac{\left[w_{i,j}\right]_{N=M=41} - \left[w_{i,j}\right]_{N=M=21}}{4^{3-1}-1}, \quad O(h^6)$$

$$\left(w_{i,j}\right)_2 = \left[w_{i,j}\right]_{N=M=81} + \frac{\left[w_{i,j}\right]_{N=M=81} - \left[w_{i,j}\right]_{N=M=41}}{4^{3-1}-1}, \quad O(h^6)$$

$$w_{i,j} = \left(w_{i,j}\right)_2 + \frac{\left(w_{i,j}\right)_2 - \left(w_{i,j}\right)_1}{4^{4-1}-1}, \quad O(h^8) \tag{27}$$

The comparison of results obtained by the FEM and semi-analytical method with and without the Richardson extrapolation technique is made in Fig. (6). As shown in this figure, the results of semi-analytical method with Richardson extrapolation appropriately converges to the results of other method. Therefore, one can conclude that this method can be used for parametric study of the elastic limit load and distribution of components of the displacement, stress and strain fields for panel with different type of geometric parameters, loading and boundary conditions.

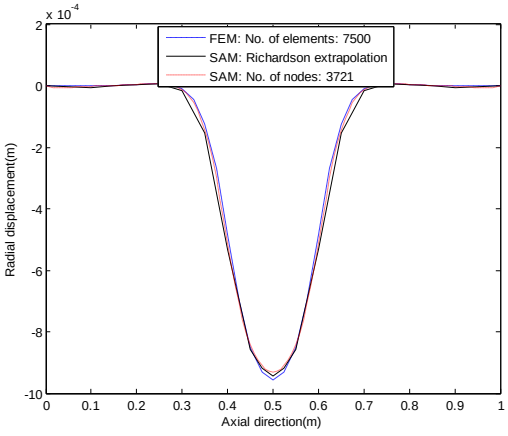

(a) Radial displacement

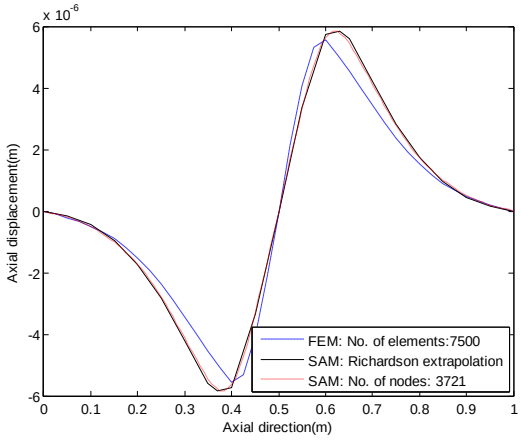

(b) Axial displacement

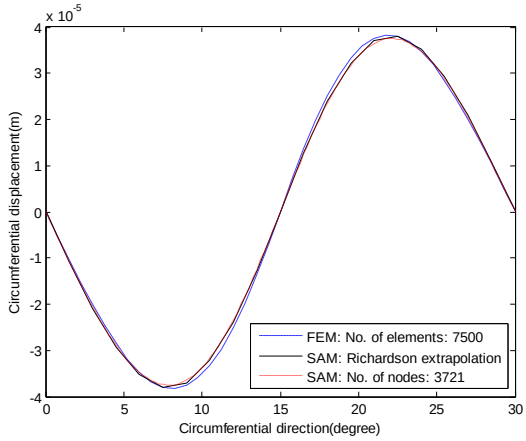

(c) Circumferential displacement

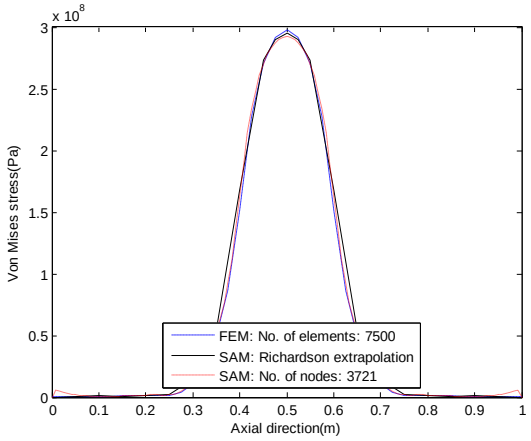

(d) Von Mises stress

Figure 6: Comparison of results of FEM, SAM without and with Richardson extrapolation, Panel model $P3$, $P_e = 9.8\,MPa$

Table 6: Number of grid nodes used for the convergence test for panel model $P3$

No. of division in X direction	No. of division in ϕ direction	No. of nodes for quarter model of panel $P3$	Δx (m)	$\Delta\phi$ (Radian)
N=21	M=21	121	0.05	0.02617
N=41	M=41	441	0.025	0.01308
N=81	M=81	1681	0.0125	0.006544

Parametric study

The main object of this section is to carry out a parametric study on effects of the geometric parameters R, ϕ_0, h on the elastic behavior of the cylindrical panel. Results of the parametric study are obtained from the verified semi-analytical method with Richardson extrapolation technique as presented in the previous section. The uniform pressure is considered to be distributed over the semi-rectangular area for all panel models listed in Table 3. Variations of the elastic limit load for proposed panel models are demonstrated in Table 7. It is found from the table that for the first three models with constant value of R and ϕ_0 and different values of h ($P1, P2, P3$), as the thickness of the panel decreases, the value of the elastic limit load decreases for the same loading range. For the last three panel model ($P3, P4, P5$), the value of h is constant and values of R and ϕ_0 are varied in such a way that $\widehat{S} = R\phi_0 = \text{constant}$. For these panel models, values of ϕ_0 and the range of loading along the ϕ direction becomes lower with the same aspect ratio. As ϕ_0 decreases or R increases, the value of the elastic limit load decreases. This means that despite reducing the range of loading along the ϕ direction, as total angle of the panel decreases the plastic flow begins at an earlier loading step.

Table 7: Elastic limit load for different panel models

Model	$p_z(x,\phi)$	Elastic limit load $P_e(MPa)$
$P1$	p_0	19.22
$P2$	p_0	13.2
$P3$	p_0	9.8
$P4$	p_0	8.6
$P5$	p_0	7.72

Variations of radial, axial and circumferential displacements for considered cylindrical panel models in the elastic limit load are shown in Fig. (7). Radial and axial components of displacement for path 1 and circumferential displacement for path 2 are shown. It is found for the first three models with different thickness ($P1, P2, P3$) that as the thickness of the panel decreases, the radial displacement of the panel increases with lower value of the elastic limit load. For the panel model with constant thickness ($P3, P4, P5$), as ϕ_0 decreases or R increases, the radial displacement increases, despite decrease in the value of the elastic limit load. According to Figs. (5 and 6), maximum von Mises stress occurs in the middle point of panel ($x = L/2$, $\phi = \phi_0/2$). This point can be considered as critical point in the cylindrical panel that in which yielding begins. As shown in Fig. (7), at this point axial and circumferential component of displacement have small values and close to zero but radial displacement has maximum values.

It is observed that variation of the displacement components of all panel models are approximately in the same range. However, the panel model $P5$ with lower value of ϕ_0 has the lowest and the panel model $P3$ with higher value of ϕ_0 and lower value of h has the highest value of axial displacement. It is also observed that the circumferential displacement of every point on all panel models increases as the thickness of the panel (h) decreases. For panel models with different total angle, as ϕ_0 decreases, the value of circumferential displacement decreases. The symmetry condition for displacement components which were implemented for simplicity of the semi-analytical method can be observed in Fig. (7). As seen in this figure, the proposed boundary conditions are in good agreement with the introduced semi-analytical method.

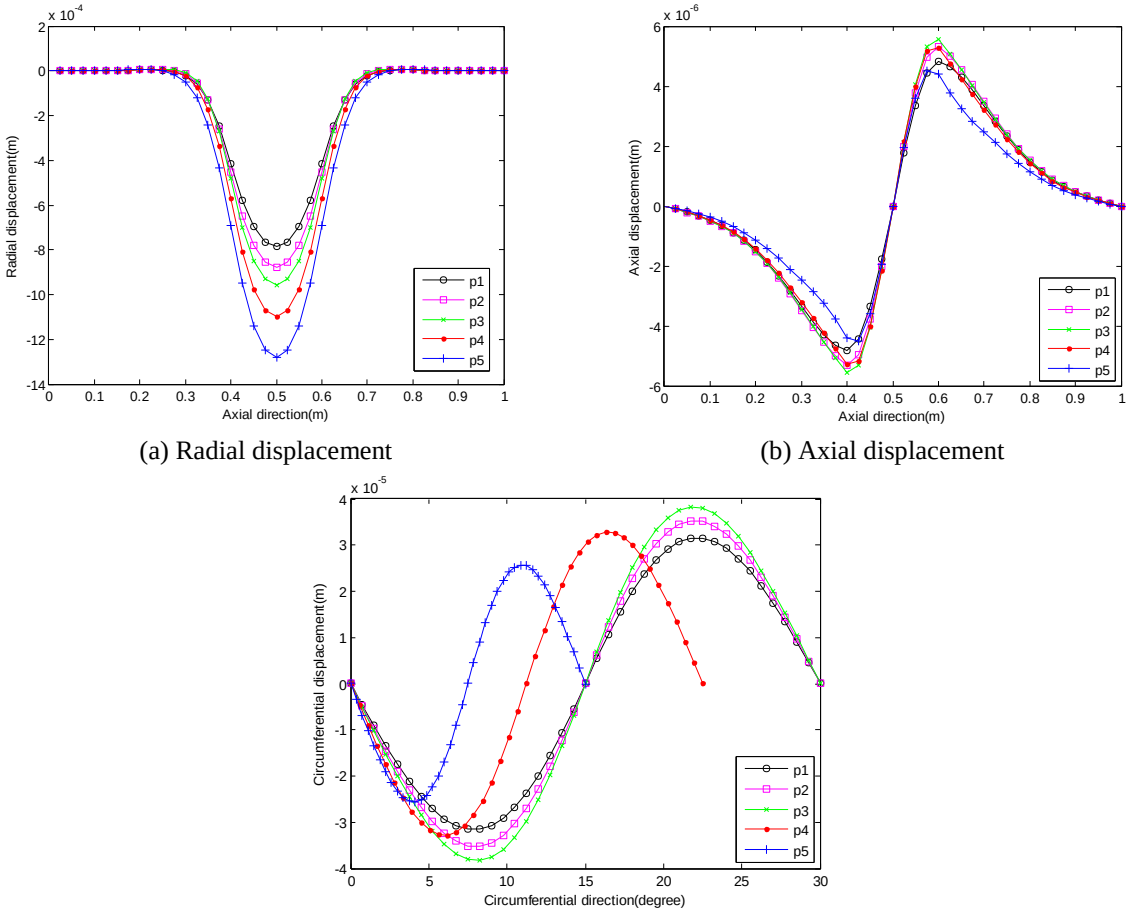

(a) Radial displacement

(b) Axial displacement

(c) Circumferential displacement

Figure 7: Variation of radial, axial and circumferential displacement for different paths on cylindrical panel at P_e in path 2.

Variations of axial and circumferential elastic strains for path 1 of the panel under uniformly distributed pressure in the elastic limit load P_e are shown in Fig. (8). As shown in this figure, the axial elastic strain along the length of the cylindrical panel have a different distribution. According to Eq. (15) definition of the axial stain is directly related to the distribution of axial and radial displacements. For the first three models with different thickness, as the thickness of the panel decreases, the axial elastic strain in the range of $0.4 \le x \le 0.6$ of panel increases with lower value of the elastic limit load. For panel model with constant thickness, as ϕ_0 decreases or R increases, the axial elastic strain decreases with lower value of the elastic limit load. It is also observed that variation of the circumferential elastic strain of all panel models are approximately in the same range. The destitution of relative stress along the path 1 can be found from the distribution of elastic strains shown in Fig. (8).

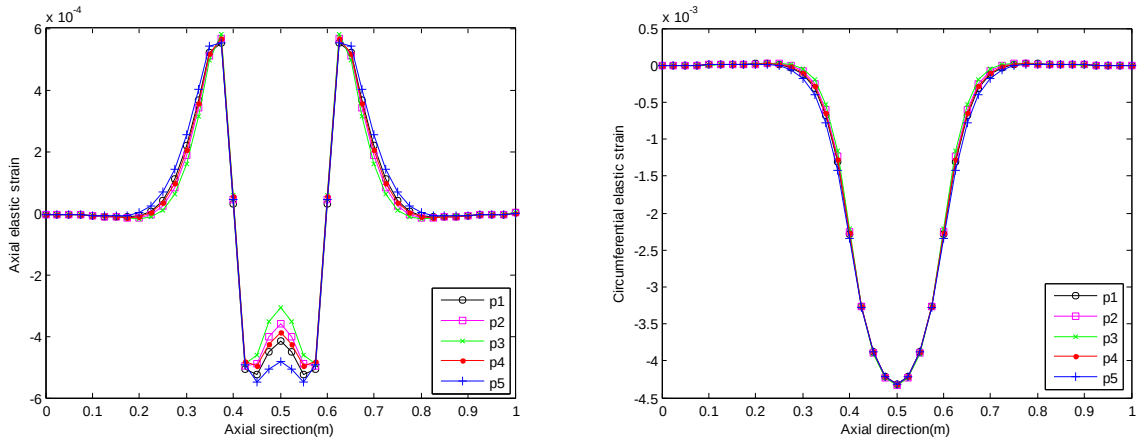

(a) Axial elastic strain (b) Circumferential elastic strain

Figure 8: Variation of axial and circumferential elastic strain for definted path 1 on cylindrical panel at p_e

The variation of von Mises stress in the cylindrical panel under uniform distributed pressure load for proposed panel models and loadings in the elastic limit load P_e are shown in Fig. (9). The results are plotted for path 1 on the cylindrical panel. Since the results are obtained for the elastic limit load, the value of maximum von Mises stress in all panel models have the same value equal to yield strength of proposed panel material. The maximum value of von Mises stress occurs at the center point of defined path or the panel in general.

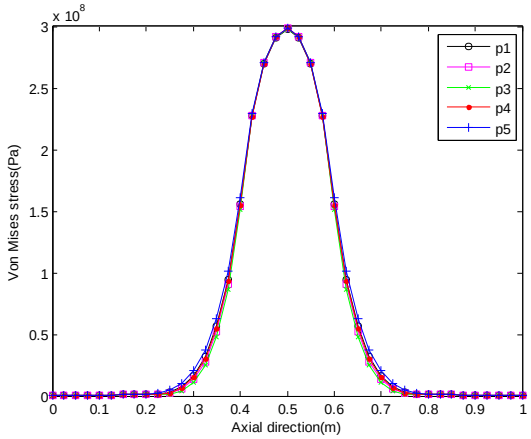

Figure 9: Variation of von Mises stress for definted path 1 on cylindrical panels at P_e

Variations of axial and circumferential stresses in the cylindrical panel under uniform distributed pressure for proposed panel models and loading ranges in the elastic limit load P_e are shown in Fig. (10). For more

clarification, results of components of the stress tensor are shown in the circumferential direction, i.e. path 2. As shown, the circumferential stress is a larger stress component for panel models in Table 3. For panel models with different thickness ($P1, P2, P3$), as h decreases the value of the axial and circumferential stress also decrease. However, the distribution of the axial and circumferential stress for panel models with constant thickness ($P3, P4, P5$), as ϕ_0 decreases, is approximately in the same range. As shown in Tables 2 and 3, values of ϕ_0 and the range of loading along the ϕ direction becomes lower with the same aspect ratio for this panel models. The result of this manner is identified in Fig. (10), which has led to sharper stress distribution in loading area. It is also interesting to note that both stresses have highest values at the center of the panel.

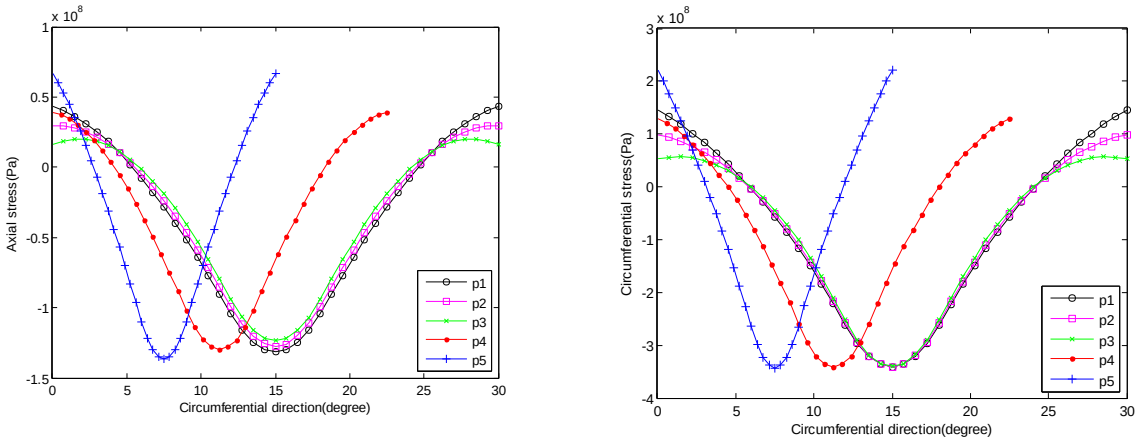

(a) Axial stress (b) Circumferential stress

Figure 10: Variation of axial and circumferential stresses for path 2 on cylindrical panel at P_e

Conclusion

Semi-analytical solutions have been presented for the elastic behavior of a thin cylindrical panel under uniformly pressure distribution. In this work, Navier method has been successfully employed to obtain the elastic limit load and distribution of displacements, stress and strain tensors in the cylindrical panel. The thin cylindrical panel is modeled using the appropriate thin shell theory. The unknown components of displacement tensor are obtained by solving the governing differential equations using the higher order finite difference method. The symmetry condition of boundary and loading of the proposed cylindrical panel is employed to efficiently reduce the size and time of computations in both finite element and semi-analytical methods. Furthermore, the Ricahrdson extrapolation technique is used to improve the accuracy and reduce the computational timing of the semi-analytical method. The verification analysis is done between FE and semi-analytical methods for uniformly pressure distribution in semi-rectangular area. Results of two methods show good agreement which validates the correctness of the presented semi-analytical model with the Richardson extrapolation technique. The parametric study is done with the semi-analytical solution employing the Richardson extrapolation technique for different values of R, ϕ_0 and h of the cylindrical panel. The results show that geometric parameter plays an important role in the deformation characteristics of cylindrical panels under the lateral pressure load. It can be concluded that the presented semi-analytical model can successfully handle the elastic analysis of the cylindrical panel and is capable of being extended into other forms of boundary, geometric and loading conditions in elastic-plastic deformations. The results of this study can be used for different pressure distribution and contact area for simulating contact that occurs between two bodies with arbitrary shape.

Reference

[1]. Sohouli. A., Goudarzi. A., and AkbariAlashti. R., (2011), Finite Element Analysis of Elastic-Plastic Contact Mechanic Considering the Effect of Contact Geometry and Material Properties, Journal of Surface Engineered Materials and Advanced Technology, 1, 125-129.

[2]. Pugliese. G., Tavares. S. M. O., Ciulli. E., and Ferreir, L. A., (2008), Rough Contacts between Actual Engineering Surfaces Part II. Contact Mechanics, Wear, 264, 1116-1128.
[3]. Perez-Gonzalez. A., Fenollosa-Esteve. C., Sanchez-Marın. F., and Vergara. M., (2008), A modified elastic foundation contact model for application in 3D models of the prosthetic knee, Medical Engineering & Physics, 30, 387–398.
[4]. Peyronnel. S.B., Wang. A., and Keer. Q.J., (2005, An extension of the Hertz theory for three dimensional coated bodies, Tribology Letters, 18, 303-314).
[5]. Ventsel. E., Krouthammer. T., (2001), Thin plates and shells: theory, analysis and applications, CRC Press,.
[6]. Sanders. J.L., (1959), An Improved First Approximation Theory for Thin Shells, NASA TR-R24.
[7]. Flugge. W., (1962), Stresses in Shells, 2nd editon, Springer-Verlag, Berlin.
[8]. Love. A. E. H., (1982), A Treatise on the Mathematical Theory of Elasticity, 1st edition, Cambridge University Press.
[9]. Timoshenko. S., Woinowsky-Krieger. S., (1985), Theory of Plates and Shells, McGraw-Hill, New York.
[10]. Niordson. F., (1985), Shell theory, Amsterdam: Elsevier Science Pub, Co.
[11]. Donnel. L. H., Beams, (1976), Plates, and Shells, McGraw-Hill, New York.
[12]. Mushtari. Kh. M., Certain generalizations of the theory of thin shells, (in Russian).
[13]. Vlasov. V. Z., (1983), General Theory of Shells and its Applications in Engineering, NASA TT F- 99, (1964).
[14]. Huble. H., (1987), Elastic-plastic cylindrical shell under axisymmetric loading- analytical solution, international journal of pressure vessel and piping, 29, 67-81.
[15]. Yi. W., Basavaraju. C., (1966), Cylindrical Shells under Partially Distributed Radial Loading, Transactions of the ASME, 118.
[16]. Tooth. S., Motashar. A., (1989), Radial loading of a cylindrical vessel through a rectangular rigid attachment, international journal of pressure vessel and piping, 37, 345-363.
[17]. Alijani. F., Aghdam. M., Abouhamze. M, (2008), Application of the extended Kantorovich method to the bending of clamped cylindrical panels, European Journal of Mechanics A/Solids, 27, 378–388.
[18]. Zahedinejad. P., Malekzadeh. P., Farid. M., Karami. G., (2010), A semi-analytical three-dimensional free vibration analysis of functionally graded curved panels, International Journal of Pressure Vessels and Piping, 87, 470-4.
[19]. Salahifar. R., Mohareb. M., (2012), Finite element for cylindrical thin shells under harmonic forces, Finite Elements in Analysis and Design , 52, 83-92.
[20]. Weicker. K,, Salahifar. R., Mohareb. M., (2010), Shell analysis of thin-walled pipes, Part I e Field equations and solution, International Journal of Pressure Vessels and Piping, 87, 402-413.
[21]. Weicker. K., Salahifar. R., Mohareb. M., (2010), Shell analysis of thin-walled pipes, Part II e Finite element formulation, International Journal of Pressure Vessels and Piping, 87, 414-423.
[22]. Ansys engineering analysis system: ver. 12. ANSYS, Inc.
[23]. AkbariAlashti R., Jafari S andHosseinipour S. J., (2015),Load Bearing Capacity of a Dented Aluminum Pipe Subjected to Internal Pressure Considering the Effect of Ductile Damage. Latin American Journal of Solids and Structures, Vo. 12 p. p. 355-384.
[24]. Jafari S., AkbariAlashti R and Hosseinipour S. J., (2014), Comparison of Ductile Fracture Models on Load Bearing Capacityof a Dented Aluminum Pipe Subjected to Internal Pressure. Arabian journal for science and engineering, Vol. 39, p. p. 8031–8049.
[25]. AkbariAlashti R., Jafari S andHosseinipour S. J., (2015), Experimental and numerical investigation of ductile damageeffect on load bearing capacity of a dented API XB pipe subjected to internal pressure. Engineering Failure Analysis, Vol. 47,p. p. 208–228.
[26]. AkbariAlashti R., Jafari S.,Hosseinipour S. J and Gorji A. H., (2013), Experimental and numerical investigation of ductile damage effect on load bearing capacity of dented pipe with different internal

pressure, wall thickness and indenter diameter. Modares Mechanical Engineering, Vol. 13, pp. 74-85, (in Persian).

[27]. AkbariAlashti R and Jafari S., (2016), The Effect of Ductile Damage on Plastic Behavior of a Rotating Disk with Variable ThicknessSubjected to Mechanical Loading.ScientiaIranica B, Vol. 23, p. p. 174-193.

[28]. Li. J., (2005), General explicit difference formulas for numerical differentiation, J. Comput. Appl. Math, 183, 29–52.

[29]. Ashok. K., Singh. B. S., (2009), Finite Difference Formulae for Unequal Sub- Intervals Using Lagrange's Interpolation Formula, Int. Journal of Math Analysis, 3, 815 – 827.

[30]. Ma. Y., Ge. Y., (2010), A high order finite difference method with Richardson extrapolation for 3D convection diffusion equation, Applied Mathematics and Computation, 215, 3408–3417 0.

[31]. Vismor .T., (2012), Matrix Algorithms,.

[32]. Burden. R. L., Faires. J. D., (2005), Numerical Analysis. 8th edition, Thomson, United Kingdom.

[33]. Maron. M. J., Lopez. R. J., (1991), Numerical Analysis: A Practical Approach, Wadsworth Publ. Co., Belmont, California.

[34]. Szilard, R., (2004), Theories and Applications of Plate Analysis, Classical, Numerical and Engineering Methods, JOHN WILEY & SONS, INC.

Appendix A

Governing equilibrium differential equations in Navier form:

$$-\frac{1}{12}\frac{Eh}{\left(\nu^2-1\right)}\left[-\frac{\partial^3 w(x,\phi)}{\partial x^3}h^2+12\frac{\partial^2 u(x,\phi)}{\partial x^2}R+12\frac{\partial^2 v(x,\phi)}{\partial x\partial\phi}\nu+12\frac{\partial w(x,\phi)}{\partial x}\nu\right]+ \tag{A-1}$$

$$\frac{E}{2(1+\nu)}\left[\frac{\partial^3 w(x,\phi)}{\partial x\partial\phi^2}R\,Ln(\frac{h+2R}{2R-h})+\frac{\partial^2 u(x,\phi)}{\partial\phi^2}Ln(\frac{h+2R}{2R-h})+\frac{\partial^2 v(x,\phi)}{\partial x\partial\phi}h-\frac{\partial^3 w(x,\phi)}{\partial x\partial\phi^2}h\right]=0$$

$$\frac{Eh}{24\left(1-\nu^2\right)}\left[\begin{array}{l}\frac{\partial^3 w(x,\phi)}{\partial x^2\partial\phi}(h^2\nu-3h^2)-12\frac{\partial^2 v(x,\phi)}{\partial x^2}(R^2\nu+\frac{1}{4}h^2\nu-R^2-\frac{1}{4}h^2)+12\frac{\partial^2 u(x,\phi)}{\partial x\partial\phi}(R\nu+R)\\ +24\frac{\partial^2 v(x,\phi)}{\partial\phi^2}+24\frac{\partial w(x,\phi)}{\partial\phi}\end{array}\right]=0 \tag{A-2}$$

$$\frac{1}{24}\frac{E}{(\nu+1)}\left[\begin{array}{l}12\frac{\partial^4 w(x,\phi)}{\partial x^2\partial\phi^2}(R^3\,Ln(\frac{h+2R}{2R-h})-12R^2h+\frac{1}{12}h^3+\frac{1}{6}h^3)+12\frac{\partial^3 u(x,\phi)}{\partial x\partial\phi^2}(R^2\,Ln(\frac{h+2R}{2R-h})-Rh)\\ -3\frac{\partial^3 v(x,\phi)}{\partial x^2\partial\phi}h^3\end{array}\right]+ \tag{A-3}$$

$$\frac{E}{\left(1-\nu^2\right)}\left[\begin{array}{l}\frac{\partial u(x,\phi)}{\partial x}Rh\nu-\frac{\partial v(x,\phi)}{\partial\phi}(R\,Ln(\frac{h+2R}{2R-h})-2h)+w(x,\phi)(2R\,Ln(\frac{h+2R}{2R-h})-h)+\\ \frac{\partial^2 w(x,\phi)}{\partial\phi^2}(R\,Ln(\frac{h+2R}{2R-h})-h)+\frac{\partial^3 v(x,\phi)}{\partial\phi^3}(R\,Ln(\frac{h+2R}{2R-h})-h)-\frac{\partial^2 w(x,\phi)}{\partial\phi^2}(2R\,Ln(\frac{h+2R}{2R-h})-2h)\\ -\frac{\partial^4 w(x,\phi)}{\partial\phi^4}(R\,Ln(\frac{h+2R}{2R-h})-h)-\frac{1}{12}\frac{\partial^4 w(x,\phi)}{\partial x^2\partial\phi^2}h^3\nu\end{array}\right]+$$

$$\frac{Eh^3}{12(\nu^2-1)}\left[-\frac{\partial^4 w(x,\phi)}{\partial x^4}R^2+\frac{\partial^3 u(x,\phi)}{\partial x^3}R+2\frac{\partial^3 v(x,\phi)}{\partial x^2\partial\phi}\nu-\frac{\partial^2 w(x,\phi)}{\partial x^2}\nu-\frac{\partial^4 w(x,\phi)}{\partial x^2\partial\phi^2}\nu\right]+p_z(x,\phi)R^2=0$$

$$0=0 \tag{A-4}$$

Appendix B

Required fourth-order finite difference formula [35]:

$$\frac{\partial f(x,\phi)}{\partial x} = \frac{-f_{i+2,j} + 8f_{i+1,j} - 8f_{i-1,j} + f_{i-2,j}}{12\Delta x} \tag{B-1}$$

$$\frac{\partial f(x,\phi)}{\partial \phi} = \frac{-f_{i,j+2} + 8f_{i,j+1} - 8f_{i,j-1} + f_{i,j-2}}{12\Delta \phi} \tag{B-2}$$

$$\frac{\partial^2 f(x,\phi)}{\partial x^2} = \frac{-f_{i+2,j} + 16f_{i+1,j} - 30f_{i,j} + 16f_{i-1,j} - f_{i-2,j}}{12\Delta x^2} \tag{B-3}$$

$$\frac{\partial^2 f(x,\phi)}{\partial \phi^2} = \frac{-f_{i,j+2} + 16f_{i,j+1} - 30f_{i,j} + 16f_{i,j-1} - f_{i,j-2}}{12\Delta \phi^2} \tag{B-4}$$

$$\frac{\partial^3 f(x,\phi)}{\partial x^3} = \frac{-f_{i+3,j} + 8f_{i+2,j} - 13f_{i+1,j} + 13f_{i-1,j} - 8f_{i-2,j} + f_{i-3,j}}{8\Delta x^3} \tag{B-5}$$

$$\frac{\partial^3 f(x,\phi)}{\partial \phi^3} = \frac{-f_{i,j+3} + 8f_{i,j+2} - 13f_{i,j+1} + 13f_{i,j-1} - 8f_{i,j-2} + f_{i,j-3}}{8\Delta \phi^3} \tag{B-6}$$

$$\frac{\partial^4 f(x,\phi)}{\partial x^4} = \frac{-f_{i+3,j} + 12f_{i+2,j} - 39f_{i+1,j} + 56f_{i,j} - 39f_{i-1,j} + 12f_{i-2,j} - f_{i-3,j}}{6\Delta x^4} \tag{B-7}$$

$$\frac{\partial^4 f(x,\phi)}{\partial \phi^4} = \frac{-f_{i,j+3} + 12f_{i,j+2} - 39f_{i,j+1} + 56f_{i,j} - 39f_{i,j-1} + 12f_{i,j-2} - f_{i,j-3}}{6\Delta \phi^4} \tag{B-8}$$

$$\frac{\partial^2 f(x,\phi)}{\partial x \partial \phi} = \frac{1}{144\Delta x\Delta \phi}\begin{bmatrix} f_{i+2,j+2} - 8f_{i+1,j+2} + 8f_{i-1,j+2} - f_{i-2,j+2} - 8f_{i+2,j+1} + \\ 64f_{i+1,j+1} - 64f_{i-1,j+1} + 8f_{i-2,j+1} + 8f_{i+2,j-1} - 64f_{i+1,j-1} + 64f_{i-1,j-1} \\ -8f_{i-2,j-1} - f_{i+2,j-2} + 8f_{i+1,j-2} - 8f_{i-1,j-2} + f_{i-2,j-2} \end{bmatrix} \tag{B-9}$$

$$\frac{\partial^3 f(x,\phi)}{\partial x \partial \phi^2} = \frac{1}{144\Delta x\Delta \phi^2}\begin{bmatrix} f_{i+2,j+2} - 16f_{i+2,j+1} + 30f_{i+2,j} - 16f_{i+2,j-1} + f_{i+2,j-2} - 8f_{i+1,j+2} \\ +128f_{i+1,j+1} - 240f_{i+1,j} + 128f_{i+1,j-1} - 8f_{i+1,j-2} + 8f_{i-1,j+2} - 128f_{i-1,j+1} \\ +240f_{i-1,j} - 128f_{i-1,j-1} + 8f_{i-1,j-2} - f_{i-2,j+2} + 16f_{i-2,j+1} - 30f_{i-2,j} + 16f_{i-2,j-1} \\ -f_{i-2,j-2} \end{bmatrix} \tag{B-10}$$

$$\frac{\partial^3 f(x,\phi)}{\partial x^2 \partial \phi} = \frac{1}{144\Delta x^2\Delta \phi}\begin{bmatrix} f_{i+2,j+2} - 16f_{i+1,j+2} + 30f_{i,j+2} - 16f_{i-1,j+2} + f_{i-2,j+2} \\ -8f_{i+2,j+1} + 128f_{i+1,j+1} - 240f_{i,j+1} + 128f_{i-1,j+1} - 8f_{i-2,j+1} \\ +8f_{i+2,j-1} - 128f_{i+1,j-1} + 240f_{i,j-1} - 128f_{i-1,j-1} + 8f_{i-2,j-1} - f_{i+2,j-2} + 16f_{i+1,j-2} \\ -30f_{i,j-2} + 16f_{i-1,j-2} - f_{i-2,j-2} \end{bmatrix} \tag{B-11}$$

$$\frac{\partial^4 f(x,\phi)}{\partial x^2 \partial \phi^2} = \frac{1}{144\Delta x^2\Delta \phi^2}\begin{bmatrix} -480f_{i,j-1} - 480f_{i,j+1} + 30f_{i,j+2} + 900f_{i,j} + f_{i-2,j-2} - 16f_{i-2,j-1} \\ +30f_{i-2,j} - 16f_{i-2,j+1} + f_{i-2,j+2} - 16f_{i-1,j-2} + 256f_{i-1,j-1} - 480f_{i-1,j} \\ -16f_{i-1,j+2} + 256f_{i-1,j+1} - 16f_{i+1,j-2} + 256f_{i+1,j-1} - 480f_{i+1,j} - 16f_{i+1,j+2} \\ +256f_{i+1,j+2} + f_{i+2,j-2} - 16f_{i+2,j-1} + 30f_{i+2,j} + f_{i+2,j+2} - 16f_{i+2,j+1} + 30f_{i,j-2} \end{bmatrix} \tag{B-12}$$